ELSEVIER

Physics of the Earth and Planetary Interiors 91 (1995) 161–176

PHYSICS OF THE EARTH AND PLANETARY INTERIORS

A very slow basal layer underlying large-scale low-velocity anomalies in the lower mantle beneath the Pacific: evidence from core phases

Edward J. Garnero [a,*], Donald V. Helmberger [b]

[a] *Earth Sciences Board and Institute of Tectonics, University of California, Santa Cruz, CA 95064, USA*
[b] *Seismological Laboratory, California Institute of Technology, Pasadena, CA 91125, USA*

Received 1 December 1994; revision accepted 8 March 1995

Abstract

A multi-phase analysis using long-period World Wide Standardized Seismograph Network and Canadian Network data has been conducted using core-phases for deep focus events from the southwest Pacific. These include SKS, S2KS, SV_{diff}, and SP_dKS. The last phase emerges from SKS near 106° and is associated with a P-wave diffracting along the bottom of the mantle. Patterns in S2KS − SKS differential travel times ($T_{S2KS-SKS}$) correlate with those in SP_dKS − SKS ($T_{SP_dKS-SKS}$). $T_{S2KS-SKS}$ values strongly depend on variations in V_S structure in the lower third of the mantle, whereas $T_{SP_dKS-SKS}$ values mainly depend on V_P structure and variations in a thin zone (100 km or less) at the very base of the mantle. Anomalously large $T_{S2KS-SKS}$ and $T_{SP_dKS-SKS}$ values (relative to the Preliminary Reference Earth Model (PREM)) are present for Fiji–Tonga and Kermadec events (recorded in North and South America), along with anomalously large SV_{diff} amplitudes well into the core's shadow. More northerly paths beneath the Pacific to North America for Indonesian and Solomon events display both PREM-like and anomalous times. A model compatible with the observations is presented, and contains a thin very-low-velocity layer at the base of the mantle that underlies the large volumetric lower-mantle low-velocity regions in the southwest Pacific. A low-velocity layer of 20–100 km thickness with reductions of up to 5–10% (relative to PREM) can reproduce $T_{SP_dKS-SKS}$ as well as SV_{diff} amplitudes. Large-scale (more than 1000 km) lower-mantle V_S heterogeneity (2–4%) can explain long-wavelength trends in $T_{S2KS-SKS}$. The exact thickness and velocity reduction in the basal layer is uncertain, owing to difficulties in resolving whether anomalous structure occurs on the source- and/or receiver-side of wavepaths (at the CMB).

1. Introduction

Departures from globally averaged 1-D reference mantle models in seismic P-wave (V_P) and S-wave (V_S) velocities (i.e. heterogeneity) can arise from regional variations in the chemical and/or thermal structure. Resolving patterns of V_P and V_S heterogeneity in the Earth's lower mantle, as well as any possible anomalous layering, may ultimately provide information on the nature and evolution of the core–mantle boundary (CMB) system.

* Corresponding author.

SSDI 0031-9201(95)03039-5

Of particular interest is structure above the CMB, from scale-lengths involving the bottom third of the lower mantle down to 10 km right at the CMB. Long-wavelength lower-mantle velocity heterogeneity (greater than 3000 km) has been used to infer the large-scale patterns of convective motions (e.g. see Forte et al., 1993) as well as viscosity structure (e.g. see King and Masters, 1992). On smaller scales of 150–300 km, both intermittent and global layering have been proposed at the base of the mantle (e.g. see Nataf and Houard, 1993; Kendall and Shearer, 1994; Krüger et al., 1995). At even smaller wavelengths (10–50 km), heterogeneity as well as CMB roughness have been proposed (e.g. see Bataille et al., 1990). Understanding and interrelating these phenomena is a present challenge in the deep Earth geosciences. More detailed information on the P- and S-wave structure of this region can ultimately help to resolve some of these issues.

When pursuing anomalous patterns in lower-mantle V_P and V_S heterogeneity, an ideal approach is to study different seismic phases on a single seismogram that separately depend on the V_P and V_S structures. Furthermore, employing a differential time analysis can minimize travel time and waveform perturbations owing to unknowns from errors in hypocentral information, as well as receiver structure. In this paper, we present such a method, which utilizes different seismic phases on a given seismogram that depend on both V_P and V_S.

The core phases SKS and SKKS (or S2KS) travel through the mantle as S waves, and convert to P waves in the core (where S2KS reflects once off the underside of the CMB), then convert back to S waves for the final mantle leg of the path. These waves depend on the structure of the outer core, as well as V_S in the lower mantle. In both forward and inverse modeling, differential times between SKS and S2KS ($T_{S2KS-SKS}$), as well as higher multiples S3KS and S4KS, have been used for determination of core structure, (e.g. see Hales and Roberts, 1971; Dziewonski and Anderson, 1981; Schweitzer, 1990; Lay and Young, 1990; Souriau and Poupinet, 1991; Tanaka and Hamaguchi, 1993; Garnero et al., 1993c). However, systematic variations in differential amplitudes and/or travel times of the SmKS (SKS, S2KS, ...) family are very sensitive to anomalous lower-mantle structure (Schweitzer, 1990; Silver and Bina, 1993; Garnero and Helmberger, 1995). In fact, $T_{S2KS-SKS}$ values are now being utilized in tomographic inversions for increased resolution of lower-mantle shear-wave heterogeneity (e.g. Liu and Dziewonski, 1994; S. Grand, personal communication, 1994). Typical epicentral distances that produce strong measurable amplitudes and times for both SKS and S2KS are 100–130°. In this distance range, adjacent SKS and S2KS CMB crossing locations are separated by roughly 700 km (see Garnero et al., 1993c). Thus, heterogeneity at scale-lengths smaller than 700 km can preferentially affect either SKS or S2KS times and amplitudes. Also, the mantle paths of SKS and S2KS are sufficiently separated to result in differing $T_{S2KS-SKS}$ predictions for different 1-D structures, i.e. if the lowermost mantle is strongly different between two models, such as strongly different vertical gradients in the D″ region, then contrasting $T_{S2KS-SKS}$ predictions may result. These issues will be discussed in detail in this paper, as SKS and S2KS are used in our analysis to gain information on the shear-wave structure at the base of the mantle.

The SP_dKS arrival, a seismic phase owing to SKS encountering the CMB with a slowness that allows for coupling with diffracted P waves (Kind and Müller, 1975; Choy, 1977; Choy et al., 1980; Garnero et al., 1993a; Helmberger et al., 1995), contains small arcs of P-wave diffraction (P_{diff}) near the SKS CMB crossing locations on both the source- and receiver-sides of the path. Fig. 1 displays the paths of SP_dKS (dashed raypaths) along with SKS and S2KS (continuous raypaths)

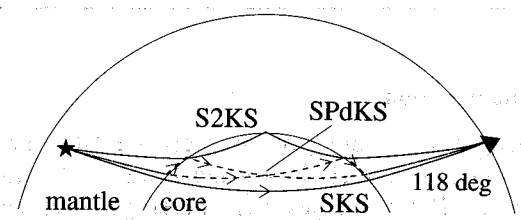

Fig. 1. Earth cross-section displaying raypaths of SKS and SKKS (continuous lines), and SP_dKS (dashed lines) for an event at 500 km depth at 118°.

Table 1
Event and station information of data used in this study

Event no.	Date (month,day,year)	Origin time (h,min,s)	Latitude (deg)	Longitude (deg)	Depth (km)	Event region
1	080564	110601	−32.22	−179.80	210	Kermadec Is.
2	081364	003115	−5.48	154.25	392	Solomon Is.
3	032467	090020	−6.01	112.33	606	Indonesia
4	012469	023303	−21.87	−179.54	587	Fiji–Tonga

for an event of 500 km depth at 118° epicentral distance. The SP_dKS phase is actually composed of an infinite set of raypaths. In Fig. 1, two end-member paths in the ray group are displayed: one raypath has the P_{diff} segment entirely on the source-side of the path, the other raypath has the

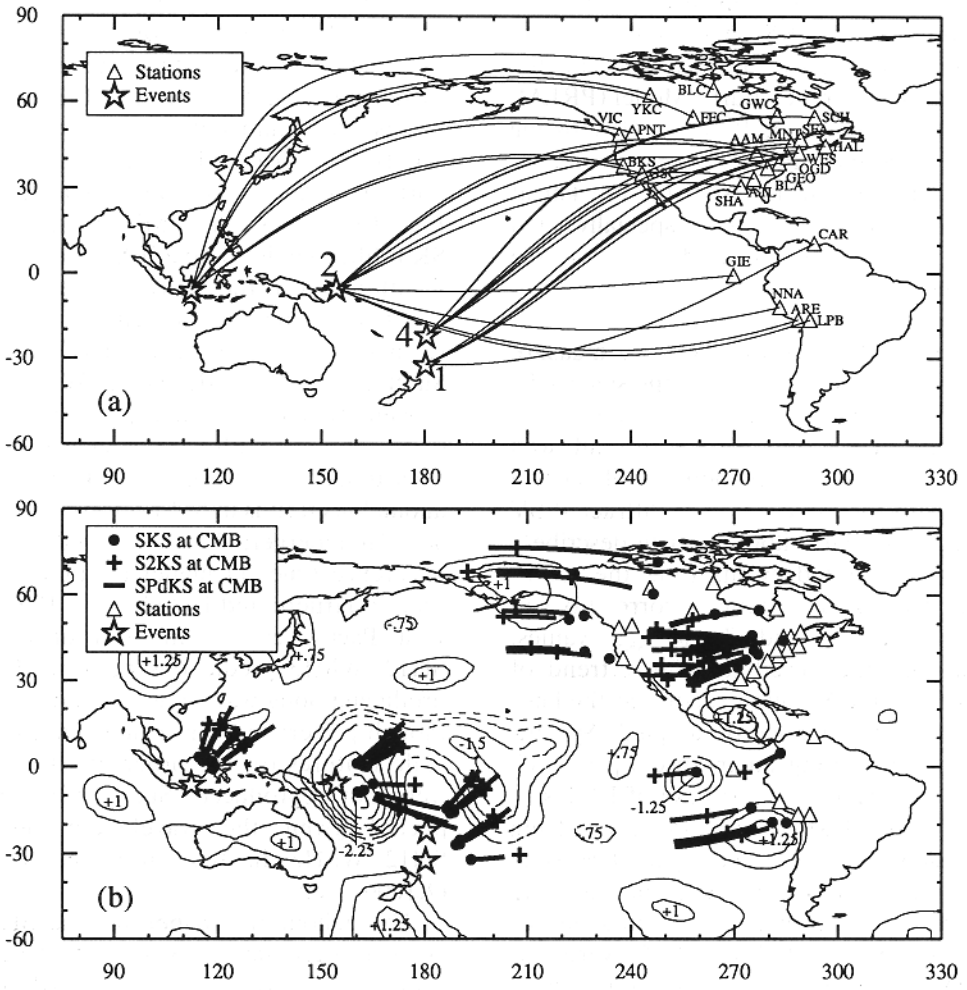

Fig. 2. (a) Great-circle raypaths projected to the Earth's surface between events (☆) and stations (△). Only paths for records with clearly measurable SKS, SP_dKS and SKKS are shown. (b) CMB crossing locations of SKS (●) and S2KS (+), and P-diffraction segments in SP_dKS. Also displayed are δV_S perturbations of magnitude greater than or equal to $|\pm 0.75|\%$ as given by model SH12_WM13 (Su et al., 1994).

P_{diff} arc solely on the receiver-side. As the P_{diff} leg continuously 'leaks' energy into the core, there exists an infinite number of paths having various lengths of small arcs of P_{diff} at both the core entrance and exit locations of SP_dKS. Because of the proximity of the SKS and SP_dKS paths, differential times between SKS and SP_dKS ($T_{SP_dKS-SKS}$) depend most strongly on V_P at the base of the mantle where the P diffraction occurs in SP_dKS (see Garnero et al., 1993a). Conversely, large-amplitude V_S heterogeneity at the base of the mantle is not expected to perturb strongly $T_{SP_dKS-SKS}$ times as the lower-mantle paths of SKS and SP_dKS are very close, especially at distances near the inception of the SP_dKS phase at 105–108° (a model-dependent distance). For example, for the 1-D Preliminary Reference Earth Model (PREM; Dziewonski and Anderson, 1981), CMB crossing locations of SKS and SP_dKS raypaths are separated by around 40 km at 110°, and 180 km at 120°. These separations are small, especially when long-period seismograms are used for study. We therefore use $T_{SP_dKS-SKS}$ values to investigate V_P structure at the very base of the mantle.

A sufficient distance range exists to measure both $T_{S2KS-SKS}$ and $T_{SP_dKS-SKS}$ on the same seismogram. From about 108° to 130° in epicentral distance, SKS, S2KS and SP_dKS are all well recorded on longitudinal components of motion (SV), along with the rapid decay of diffracted SV waves (SV_{diff}). In what follows, we will describe a sample of well-recorded events from the southwest Pacific that display systematic correlations in anomalous $T_{S2KS-SKS}$ and $T_{SP_dKS-SKS}$ values. These times are then used to infer a trend of correlation of P- and S-wave structure at the base of the mantle for the regions sampled. Specifically, a scenario relating an intense V_P and V_S low-velocity zone (LVZ) at the base of D″ (as in Garnero et al. (1993a)) to large-scale overlying features of slower-than-average V_S (and possibly V_P) is discussed. The lower mantle beneath the western and southwestern Pacific is pursued because it is a region depicted by both forward and inverse studies as having very anomalous slower than average structure beneath the central–southwest Pacific, and faster than average circum-Pacific velocities.

2. SKS, S2KS, and SP_dKS data set

Data from four mid- and deep-focus events of the southwest Pacific recorded at World Wide Standardized Seismographic Network (WWSSN) and Canadian Network stations have been utilized. Table 1 lists the hypocentral information of these events. The older archive data has been utilized owing to the at present unsurpassed station coverage across North America for the necessary large distance ranges. Long-period (10–20 s) SV components of the data have been obtained through optically scanning and digitizing the original paper records, then rotating them into the SV and SH components of motion.

Great circle wave paths projected to the Earth's surface are displayed in Fig. 2(a), along with the events (stars) and stations (triangles). These four events have wave paths that sample very different portions of the lower mantle beneath the Pacific. Fig. 2(b) displays the CMB crossing locations of SKS (filled circles) and S2KS (crosses), the arcs of P diffraction in the SP_dKS phase (thick continuous line segments), as well as contours of the stronger V_S heterogeneity in D″ as reported by Su et al. (1994) (Model SH12_WM13). Only heterogeneity having magnitude $\delta V_S > |\pm 0.75|\%$ (with respect to PREM) is shown in the figure. This model has proven satisfactory in matching anomalous trends in S–SKS travel times (Garnero and Helmberger, 1993), as well as anomalous difference times in higher multiple SKS (SmKS) times (Garnero and Helmberger, 1995) for southwest Pacific events. In both of those studies SH12_WM13 predictions performed well in reproducing long-wavelength trends in the data, though patterns in travel times owing to smaller-scale features (of the order of 100 km or more) were not reproduced. Such differences are expected given the wavelength resolution of SH12_WM13 in the lower mantle, of order $O(1000 + \text{km})$.

Throughout this paper we use SH12_WM13 as a representative aspherical structure. This choice is somewhat arbitrary, though our purpose is not to test the model as much as it is to qualitatively compare our measurements to general long-wavelength predictions. We will

demonstrate the correlation of patterns of large scale heterogeneity in SH12_WM13 with systematic trends in the observed $T_{S2KS-SKS}$ and $T_{SP_dKS-SKS}$ times.

3. Observed and synthetic waveforms

We have computed synthetic seismograms for comparison with the observations by the reflectivity method (e.g. see Kind and Müller, 1975). The synthetics have been convolved with a source-time function trapezoid and the appropriate long-period instrument. The trapezoid dimensions were chosen to produce the best fit between synthetics and data for the SKS waveforms (beyond distances displaying SP_dKS interference with the first pulse of SKS). This source–time function is then used for all records of the event being modeled. Fig. 3 shows long-period WWSSN

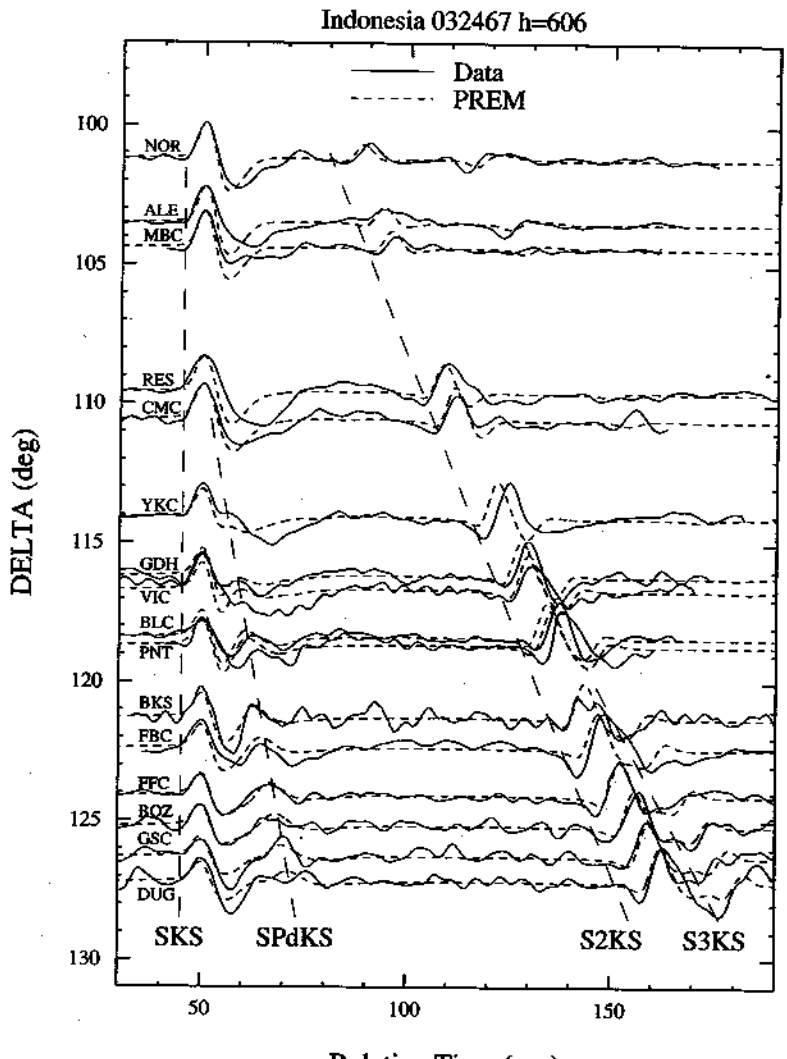

Fig. 3. SV components of observations (continuous traces) and reflectivity PREM predictions (dashed traces) for the Indonesian event.

observations from the Indonesian event (continuous traces) along with PREM long-period WWSSN reflectivity predictions (dashed traces). Synthetics and observations have been normalized in time and amplitude to the SKS arrival. The onsets SKS, S2KS, and S3KS, and the peak of SP_dKS are indicated by long dashed lines. The reflectivity method includes the $\pi/2$ phase shift of S2KS with respect to SKS (e.g. see Choy and Richards, 1975). The PREM predictions well match the observations for SKS, SP_dKS and S2KS with a few notable exceptions. Stations YKC (Yellowknife, Northwest Territory), BLC (Baker Lake, Northwest Territory) and PNT (Pentitcon, British Columbia) all possess larger $T_{S2KS-SKS}$ values than PREM. These records also display SP_dKS waveform distortions (YKC) and large $T_{SP_dKS-SKS}$ separations (BLC and PNT). On average, however, PREM predictions provide a good match to the Indonesian data, which is what might be expected from the absence of strong lower-mantle heterogeneity as predicted by

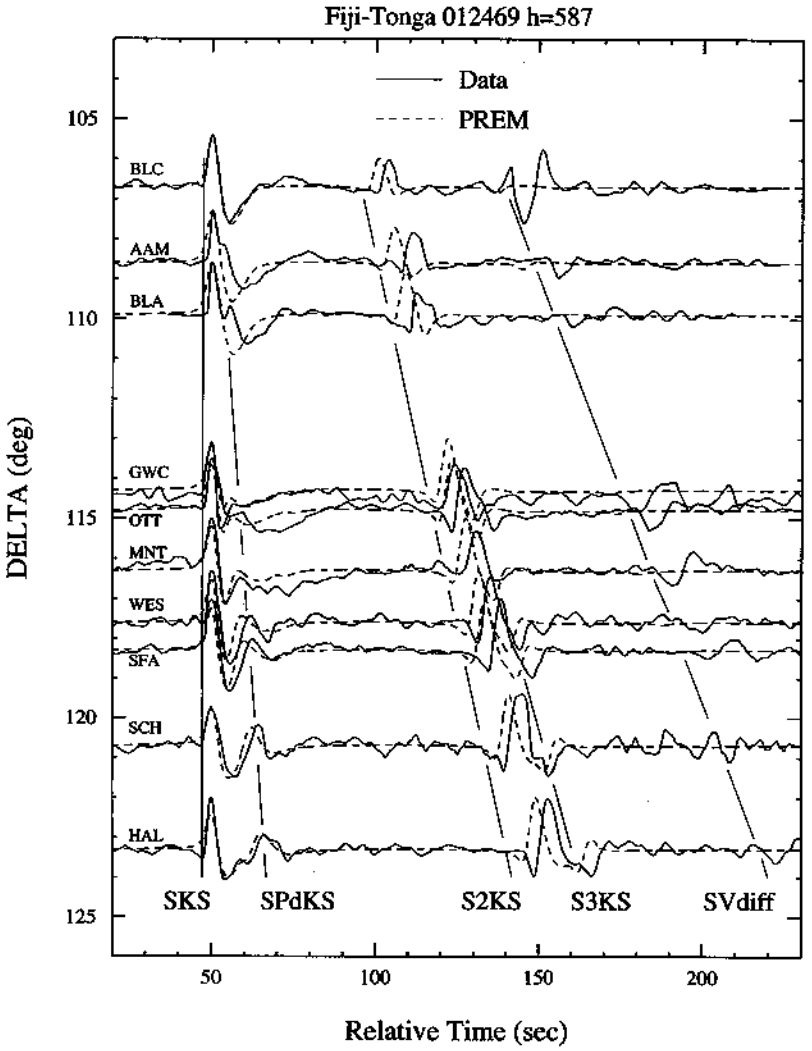

Fig. 4. SV components of observations (continuous traces) and reflectivity PREM predictions (dashed traces) for the Fiji–Tonga event.

SH12_WM13 for these paths (Fig. 2(b)). The behavior of large $T_{SP_dKS-SKS}$ values accompanying large $T_{S2KS-SKS}$ values, and 'normal' or PREM-predicted $T_{SP_dKS-SKS}$ values accompanying PREM-predicted $T_{S2KS-SKS}$ values is a point we will repeatedly exploit in this paper.

Data and synthetics for the Fiji–Tonga event are displayed in Fig. 4. In strong contrast to the Indonesian data of Fig. 3, the Fiji–Tonga data display very anomalous $T_{S2KS-SKS}$ values, as well as anomalously delayed SP_dKS arrivals relative to SKS. This event displays $T_{S2KS-SKS}$ anomalies greater than 5 s, which is in agreement with those reported by Schweitzer and Müller (1986) and Schweitzer (1990) for the same path geometry. $T_{SP_dKS-SKS}$ values are separated by several seconds more than PREM (as presented by Garnero et al. (1993a)). Observed $T_{SP_dKS-SKS}$ values are larger than PREM predictions, which corresponds to a smaller distance where SP_dKS pulses are first observable. For example, Stations AAM (Ann Arbor, Michigan, 108.6°) and BLA (Blacksburg, Virginia, 109.9°) display strong SP_dKS arrivals in the shoulder of the SKS (owing to a several second delay in SP_dKS relative to SKS), a phenomenon not apparent in PREM synthetics until 113–114°.

Also apparent in Fig. 4 are anomalously strong SV_{diff} waves relative to PREM. These arrivals are also delayed by 8–10 s relative to SKS (Garnero and Helmberger, 1993). This can be seen, for example, at AAM where there is a small amplitude SV_{diff} arrival in the synthetics 10 s in front of the large observed SV_{diff}. As the diffraction in SV_{diff} occurs in a lower-mantle region that is slightly different from that traversed by SKS, S2KS and SP_dKS, we will concentrate on the core wave data.

To emphasize further the trend that anomalous S2KS – SKS separations are accompanied by anomalous delays in SP_dKS relative to SKS, single records from three of the events in Table 1 are shown in Fig. 5(a) (continuous traces) along with reflectivity PREM predictions (dashed traces) for the appropriate distances and source depths. The predicted $T_{S2KS-SKS}$ values vary owing to source depth differences (e.g. comparing the Kermadec synthetic with the Indonesia synthetic). All three records are near 110°. This is a critical distance for observing SP_dKS: it is just before distances where SP_dKS is first detectable for models having PREM-like D″ velocities. Models with pronounced low-velocity zones at the base of D″ (5% reductions and larger), however, predict SP_dKS to be strongly developed in the shoulder of SKS at this range (Garnero et al., 1993a). Fig. 5(b) shows six recordings of SKS and SP_dKS of the Fiji–Tonga event. Also included in the figure are synthetics for a model having a 5% linear reduction from PREM in the bottom 100 km of the mantle. These synthetics display an anomalously delayed SP_dKS arrival, as present in

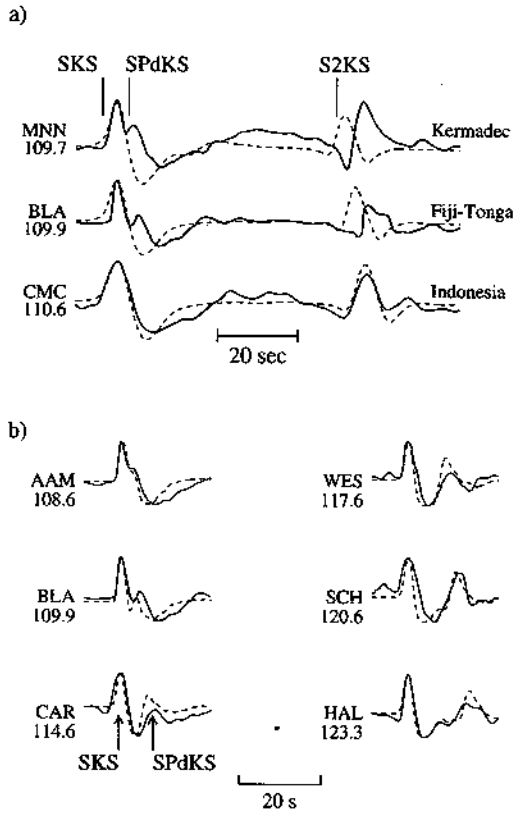

Fig. 5. (a) Observations near 110° for three events (continuous traces) compared with reflectivity predictions for PREM (dashed traces). The Kermadec and Fiji–Tonga records display anomalous behavior in both T_{S2-SKS} and $T_{SP_dKS-SKS}$, whereas the Indonesia record is well modeled by PREM. (b) Observed SKS and SP_dKS waveforms for the Fiji–Tonga event (continuous traces) and reflectivity synthetics (dashed traces).

the observations. An even larger reduction in V_P is necessary to fit the BLA record, for example. This illustrates how lateral variations in V_P in the low-velocity basal layer are necessary to model all the data. Synthetics produced for various D″ discontinuity structures do not produce any noticeable SP_dKS distortions; this is due to the relative insensitivity of P_{diff} in LP WWSSN SP_dKS arrivals to structure much over 100 km above the CMB. Records WES and HAL display reduced SP_dKS/SKS amplitude ratios compared with synthetics. Such reductions in amplitude result if the LVZ layer only occurs on one side of the wavepaths (e.g. on the source-side beneath the SH12_WM13 large-scale low-velocities). The issue of lateral variations in the basal layer, and resulting SP_dKS amplitude reductions and distortions have been explored elsewhere (Garnero and Helmberger, 1994).

For the Kermadec and Fiji–Tonga records in

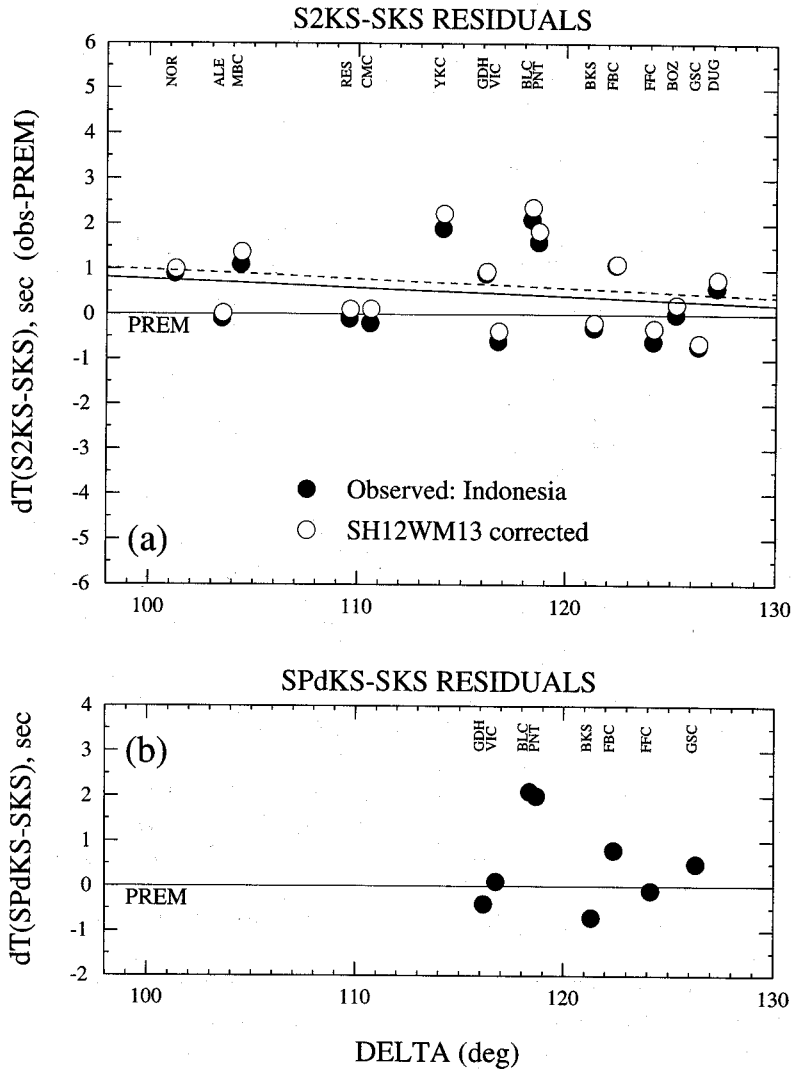

Fig. 6. (a) Observed (●) and SH12_WM13 corrected (○) $\delta T_{S2KS-SKS}$ residuals (with respect to PREM) plotted as a function of epicentral distance, for data of the Indonesian event. The non-zero continuous and dashed lines correspond to least-squares fits to the observed and corrected residuals, respectively. (b) Observed $\delta T_{SP_dKS-SKS}$ residuals.

Fig. 5(a), anomalous SP_dKS arrivals are apparent (equivalently seen as large $T_{SP_dKS-SKS}$ values). Also readily apparent for these two records are large $T_{S2KS-SKS}$ values in comparison with PREM predictions. The Indonesian record, however, has no SP_dKS waveform anomaly. This record also displays no $T_{S2KS-SKS}$ anomaly. Implications of the correlation between $T_{SP_dKS-SKS}$ and $T_{S2KS-SKS}$ values will be explored in the following sections.

4. Travel times

In this section the differential travel times $T_{S2KS-SKS}$ and $T_{SP_dKS-SKS}$ are analyzed. The former have been calculated by Hilbert transforming SKS (see Choy and Richards, 1975) to be in proper phase with S2KS, then cross-correlating the traces to obtain a difference time, and the latter times were calculated by determining the difference between the peak times of SKS and

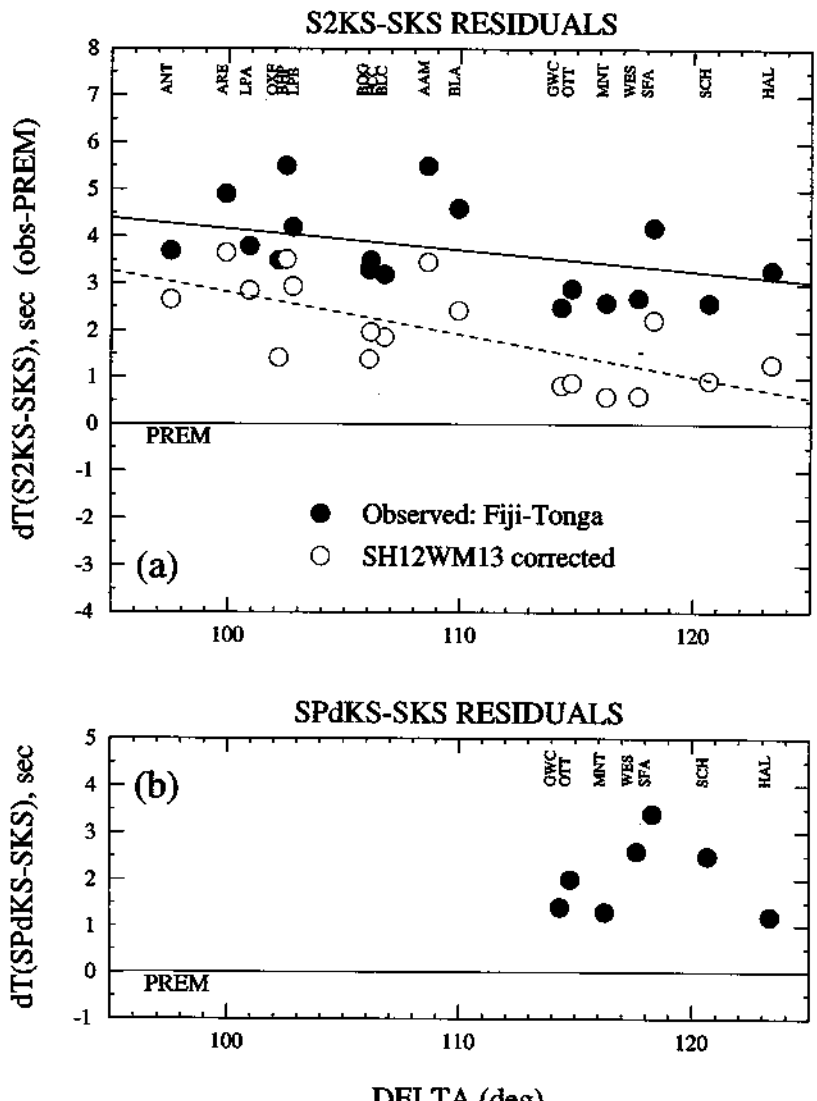

Fig. 7. Same as in Fig. 6, except for Fiji–Tonga data for (a) $\delta T_{S2KS-SKS}$ and (b) $\delta T_{SP_dKS-SKS}$.

SP_dKS (Garnero et al., 1993a). The above methods were identically applied to data and synthetics, where the synthetics were constructed for the appropriate distances and source depths assuming PREM. Predictions from PREM were subtracted from observed $T_{S2KS-SKS}$ and $T_{SP_dKS-SKS}$ values to construct the differential travel time residuals $\delta T_{S2KS-SKS}$ and $\delta T_{SP_dKS-SKS}$, respectively. SP_dKS arrivals for PREM become distinct peaks later in time than SKS at distances greater than around 114°, so that $\delta T_{SP_dKS-SKS}$ residuals could only be calculated for distances greater than 114°. However, waveform distortions of the combined SKS and SP_dKS pulse are obvious at the shorter distances for some of the traces (Figs. 5(a) and 5(b)).

The residual times $\delta T_{S2KS-SKS}$ and $\delta T_{SP_dKS-SKS}$ are presented in Figs. 6(a) and 6(b), respectively, for the Indonesian event (filled circles). $\delta T_{S2KS-SKS}$ values for this path geometry (Fig. 6(a)) mostly scatter within ± 1 s of PREM predictions (zero line). The notable exceptions are Stations YKC, BLC, and PNT, which have SKS and S2KS separated by around 2 s more than PREM. As mentioned above, these stations also display SP_dKS anomalies, which are apparent in Fig. 6(b). All the data for this event average near +0.5 s, as seen from the continuous line in Fig. 6(a), which is the least-squares fit to the points. The $\delta T_{S2KS-SKS}$ values were corrected for predictions through the 3-D model SH12_WM13 (Fig. 6(a), open circles). As SH12_WM13 does not predict strong heterogeneity for the Indonesian paths, the corrected $\delta T_{S2KS-SKS}$ times differ only slightly from the observed residuals. This is also apparent from comparing the least-squares fit with the raw residuals and the corrected residuals (dashed line). As SP_dKS phases involve P-wave diffraction, we have not attempted to correct $\delta T_{SP_dKS-SKS}$ residuals with an S-wave heterogeneity model. Fig. 6(b) shows how the $\delta T_{SP_dKS-SKS}$ residuals (other than BLC and PNT) are close to zero, suggesting that the base of the mantle V_P structure in PREM is adequate on average in modeling data from this event.

In contrast, the Fiji–Tonga data of Fig. 4 differ greatly from the Indonesian data of Fig. 3. The anomalous travel times from the Fiji–Tonga event are summarized in Fig. 7. The anomalously large $\delta T_{S2KS-SKS}$ (Fig. 7(a)) and $\delta T_{SP_dKS-SKS}$ (Fig. 7(b)) residuals are readily apparent. The least-squares fit to the observations (continuous line) averages between 3 and 4 s. The corresponding $\delta T_{SP_dKS-SKS}$ residuals are also large, and average around 2 s. Wavepaths for this source–receiver geometry traverse a large LVZ at the base of the mantle, as predicted by SH12_WM13 (Fig. 2(b)). For this event, SH12_WM13 predicts that S2KS paths cross the CMB in slower material than SKS, which results in an increased separation between SKS and S2KS. This results in a predicted $T_{S2KS-SKS}$ anomaly of the same sign as that observed. For this reason, corrected $\delta T_{S2KS-SKS}$ values (open circles, Fig. 7(a)) are closer to the PREM zero line than the raw data (see also the least-squares fit dashed line to the corrected data).

SH12_WM13 underpredicts the size of these observed $\delta T_{S2KS-SKS}$ anomalies for this path geometry. However, a more recent version of SH12_WM13 includes T_{S-SKS} and $T_{S2KS-SKS}$ values (Liu and Dziewonski, 1994) which improves lowermost-mantle resolving power. Using the modified model results in larger lower-mantle δV_S perturbations (up to around 4% rather than 2.5%). This would help further to correct observed $\delta T_{S2KS-SKS}$ values in Fig. 7(a) to that predicted by PREM (zero line). Our main focus, however, is to show the correlation of the anomalous $\delta T_{S2KS-SKS}$ and $\delta T_{SP_dKS-SKS}$ values.

The $\delta T_{S2KS-SKS}$ and $\delta T_{SP_dKS-SKS}$ residuals for all four events are summarized in Fig. 8. In both panels, the horizontal and vertical axes correspond to $\delta T_{S2KS-SKS}$ and $\delta T_{SP_dKS-SKS}$ residuals, respectively, with respect to PREM. A ± 1 s error bar has been added to the symbols to emphasize that some error may arise in the cross-correlation scheme, as well as from source mislocations. Our picking errors do not exceed ± 0.5 s, but small timing artifacts ($\pm \frac{1}{4}$ s) might be introduced in the digitization process. Hence we choose ± 1 s error bars to represent our possible cumulative errors conservatively. Fig. 8(a) displays the raw residuals with different symbols representing the different events. The pattern of residuals shows that large $\delta T_{S2KS-SKS}$ values accompany large

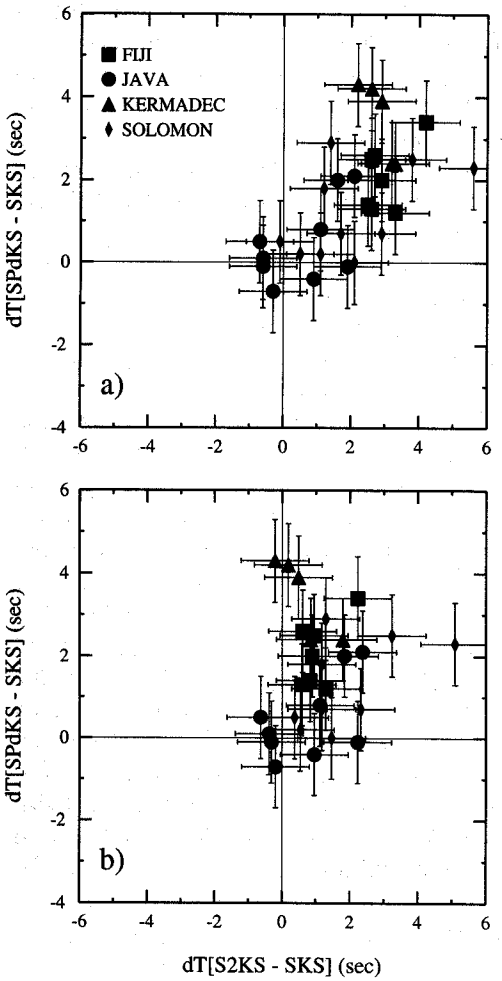

Fig. 8. Plots of $\delta T_{SP_dKS-SKS}$ vs. $\delta T_{S2KS-SKS}$ for the four events of Table 1. (a) The raw data. (b) $\delta T_{S2KS-SKS}$ residuals corrected for SH12_WM13.

$\delta T_{SP_dKS-SKS}$ values. Fig. 8(b) is the same as in 8(a), with the addition of $\delta T_{S2KS-SKS}$ residuals being corrected for SH12_WM13 predictions. The trend in the corrected times is shifted closer to the $\delta T_{S2KS-SKS} = 0$ axis. These times firmly establish the trend of correlated $T_{S2KS-SKS}$ and $T_{SP_dKS-SKS}$ behavior for the source geometries in Fig. 2. We now explore the possible implications of such a correlation.

5. Interpretation and discussion

Our basic observation is that anomalous $T_{S2KS-SKS}$ values generally exist when anomalous $T_{SP_dKS-SKS}$ are present. In interpreting these data, we assume that a possible misfit in the outer core structure of PREM does not contribute to our anomalies. Garnero et al. (1993c) showed that SmKS predictions from the PREM outer core structure provide a good fit to observations for the Indonesian path geometry of Fig. 2, with the exception of the outermost 50 km of the core, which only very slightly affects SKS, S2KS, and SP_dKS for the ranges of this study. We also assume that the core does not possess lateral heterogeneity, as mantle heterogeneity can account for the long-wavelength patterns in the observed anomalies. Also, dynamical arguments suggest that heterogeneity in the rapidly convecting core cannot be sustained (Stevenson, 1987). If outer core heterogeneity does exist, seismic resolution of such remains elusive at present, owing to uncertainties in mantle structure (Garnero and Helmberger, 1995).

As SKS arrives before S2KS, anomalously large $T_{S2KS-SKS}$ values imply that either SKS is fast or S2KS is slow (or both). Similarly, anomalously large $T_{SP_dKS-SKS}$ values imply that SKS is fast and/or SP_dKS is slow. Therefore anomalously fast SKS waves and 'normal' S2KS and SP_dKS arrivals can account for the observed $T_{S2KS-SKS}$ and $T_{SP_dKS-SKS}$ correlation. For this reason, it is necessary to review the absolute SKS times (T_{SKS}). Unfortunately, the origin times for older events may be uncertain owing to mislocation in depth. As an attempt to circumvent this, for a given event the mean of all T_{SKS} delays (with respect to PREM) was removed from each individual observation to yield an adjusted T_{SKS} delay (δT_{SKS}). These adjusted times can be useful when compared with $\delta T_{S2KS-SKS}$ residuals; if SKS is anomalously fast at a given station (compared with the average of T_{SKS} values for the given event), then δT_{SKS} will be negative and $\delta T_{S2KS-SKS}$ will be correspondingly large. Hence if SKS is responsible for the large observed $T_{S2KS-SKS}$ values, then δT_{SKS} and $\delta T_{S2KS-SKS}$ values should correlate. Fig. 9(a) displays δT_{SKS} values for our data plotted against the raw $\delta T_{S2KS-SKS}$ residuals. No clear trend between δT_{SKS} and $\delta T_{S2KS-SKS}$ is evident, for all the data nor on an event-by-event basis. Fig. 9(b) plots SH12_WM13 synthetic predictions for δT_{SKS} and

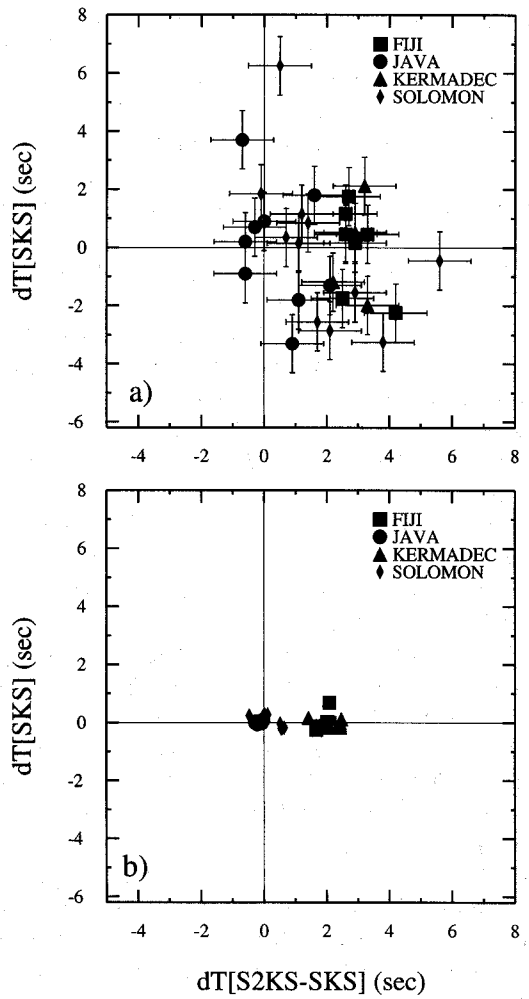

Fig. 9. Relative SKS delays δT_{SKS} (see text) vs. $\delta T_{S2KS-SKS}$ residuals for (a) observations, and (b) synthetic predictions of model SH12_WM13.

$\delta T_{S2KS-SKS}$ (i.e. purely predictions through the model; no data or data corrections are involved). This model does not predict relatively fast SKS arrivals to accompany large $\delta T_{S2KS-SKS}$ residuals. In fact, for the path geometries in Fig. 2, calculated T_{SKS} anomalies through SH12_WM13 do not span much more than a 1 s range. Although this reasoning does not preclude relatively fast SKS waves contributing to our $T_{S2KS-SKS}$ and $T_{SP_dKS-SKS}$ anomalies, it argues against such as the major source of the observed anomalies.

The most effective way to increase $T_{SP_dKS-SKS}$ predictions to match anomalous SP_dKS waveform and travel times observations is to reduce V_P right at the base of the mantle (Garnero et al., 1993a; Garnero and Helmberger, 1994). This delays the diffracted P legs of the SP_dKS arrival. There are some inherent trade-offs in the intensity of the LVZ in V_P and the thickness over which the LVZ occurs, as well as whether the LVZ is a gradient linear reduction from the reference model, or a discontinuous LVZ layer. Also, the inherent uncertainty between the source- and receiver-side's contribution to SP_dKS anomalies is present. Nonetheless, Garnero and Helmberger (1994) demonstrated that perturbing V_P in D″ on just one side of the model, e.g. the source-side, produces excellent fits to the data for the anomalous data of the southwest Pacific. This can be accomplished with a discontinuous LVZ in V_P, for example, on the source-side of SP_dKS wavepaths, with velocities reduced by as much as 5–10% from PREM over a zone of 20–50 km thickness. Less extreme reductions are necessary if one assumes a 1-D structure in the modeling procedure. However, as SH12_WM13 in Fig. 2(b) suggests, we would not expect a 1-D structure to be realistic for these paths. $T_{SP_dKS-SKS}$ values are less sensitive to V_P structure above such a zone of low velocities. Also, owing to closeness of SKS and SP_dKS paths, V_S heterogeneity is not expected to perturb these times significantly.

$T_{S2KS-SKS}$ values, on the other hand, can be perturbed by much larger-scale lower-mantle features, owing to increased wavepath separation in the lowermost mantle. Nonetheless, it is difficult to produce large $T_{S2KS-SKS}$ perturbations from 1-D modeling efforts, unless V_S is strongly reduced over a depth range in the lower mantle of several hundred kilometers. Three-dimensional structure is more effective in perturbing, say, S2KS relative to SKS, resulting in $T_{S2KS-SKS}$ perturbations comparable in amplitude with observations (Fig. 2(b) suggests such variations).

Conversely, $T_{S2KS-SKS}$ values do not have strong resolving power of structure right at the base of the mantle. The presence of SV_{diff} out to

large distances, however, is evidence for an LVZ in V_S (e.g. Lay and Young, 1991; Vinnik et al., 1995). In our reflectivity modeling experiments, a 5–6% linear gradient reduction from PREM in the bottom 50–100 km of the mantle, or a 5–10% discontinuous reduction from PREM in the bottom 20–30 km of the mantle can match the anomalously large SV_{diff} amplitudes. Our experiments also indicate how low Q can affect amplitudes of SV_{diff}, making difficult subsequent V_S structural interpretations. Further 2-D heterogeneity must be invoked to match the anomalous SV_{diff}–SKS difference times, as discussed above in Fig. 4.

In a fairly straightforward fashion, we can produce $T_{S2KS-SKS}$ and $T_{SP_dKS-SKS}$ reflectivity predictions for various classes of V_P and V_S LVZs, to plot with the data in Fig. 8. For example, a 3–4 s delay in SP_dKS with respect to SKS can be produced from a 5–6% LVZ in V_P distributed over 100 km of the lowermost mantle. Similarly, an 8–10% discontinuous reduction from PREM V_P over 30 km at the base of the mantle can do the same. This magnitude of anomaly matches the largest $\delta T_{SP_dKS-SKS}$ residuals in Fig. 8(a). Matching the largest observed $\delta T_{S2KS-SKS}$ residuals through 1-D modeling can be accomplished only with large V_S reductions over extended lower-mantle depths. For example, an 8% reduction in V_S over the lowermost 600 km of the mantle produces $\delta T_{S2KS-SKS}$ of approximately 3 s. Such large V_S reductions are probably unreasonable, as they should have been detected in the tomographic studies. This emphasizes the point that 3-D modeling is necessary to match the $\delta T_{S2KS-SKS}$ residuals.

Data with anomalously delayed S2KS relative to SKS are observed when SP_dKS is also delayed. A velocity model scenario compatible with these observations has the following characteristics:

(1) a strong low-velocity layer in V_P at the base of the mantle with a reduction from PREM of 5–10% over 20–100 km. This feature satisfies the $T_{SP_dKS-SKS}$ observations.

(2) To reproduce the strong SV_{diff} amplitudes, a strong low-velocity layer in V_S right at the base of the mantle of a similar magnitude and thickness to that in (1) is preferred. This is less constrained owing to lateral averaging of structure by SV_{diff} and also the trade-off between Q and structure in amplitudes of SV_{diff}.

(3) Large-scale LVZ in V_S in the lower mantle on the source-side of the anomalous $T_{S2KS-SKS}$ paths. As depicted by SH12_WM13, this feature may be several thousand kilometers wide, and extend several hundred kilometers up from the CMB. As shown in Fig. 2(b), this slow feature can preferentially delay S2KS more than SKS (for Events 1 and 4), producing the observed $\delta T_{S2KS-SKS}$ anomalies. Unfortunately, we are unable to make any statements concerning the V_P structure far above the CMB, as our data are not sensitive to such. However, tomographic inversions for aspherical V_P structure (e.g. Dziewonski, 1984) also display large lower than average velocities for this same region. Therefore a large LVZ for V_P, as in (3) above, although not constrained by our data, may be appropriate.

A more complete data search is necessary to document the global behavior of $T_{S2KS-SKS}$ and $T_{SP_dKS-SKS}$ correlations. Our preliminary finding is that the large volumetric V_S low velocities beneath the southwest Pacific (as depicted by SH12_WM13) are underlain by a very low P- and S-velocity basal layer. It will be necessary to determine if this trend is always observed for large volumetric LVZs, such as that beneath Africa as seen in SH12_WM13 (see Su et al., 1994). The preliminary results discussed by Garnero et al. (1993a) would seem to confirm our hypothesis.

An inherent uncertainty in modeling D″ structure is the possibility of anisotropy at the base of the mantle. Observations of split SH and SV waves, as well as large SV_{diff} amplitudes, have been used to propose anisotropy as a possibility in the D″ region (Vinnik et al., 1989, 1995; Lay and Young, 1991; Maupin, 1995). No SH–SV splitting is observed for the large SV_{diff} arrivals in Fig. 4. However, this is the same path geometry as given by Vinnik et al. (1995) and Maupin (1995), who claimed that anisotropy may be contributing to large SV_{diff} amplitudes. More research is necessary to resolve this issue.

For the regions sampled by our data, correlated patterns of V_P and V_S heterogeneity are compatible with the correlated $T_{S2KS-SKS}$ and

$T_{SP_dKS-SKS}$ times of Fig. 8. Wysession et al. (1992) argued for both regions of correlated and anticorrelated D″ V_P and V_S structure for various regions around the globe. Their regions of study do not overlap with ours, so a direct comparison is not possible. Future research with the SKS wavetrain for other regions will aid in corroborating earlier studies for other regions.

With the implementation of the various broadband networks across North America, we are rapidly approaching the station coverage of the combined WWSSN and Canadian station networks. Broadband data will permit analysis of the frequency dependence of SP_dKS and SV_{diff} behavior, which is undoubtedly a model-dependent feature. Analysis of other types of data, such as core-grazing short-period P waves (e.g. see Ruff and Helmberger, 1982; Young and Lay, 1989), will also provide strong constraints on the depth extent, gradient and structure of the LVZ structure at the base of the mantle.

As the details of the structure of the thin low-velocity basal layer are uncertain, it is difficult at this time to hypothesize the nature of the source of the low velocities. It remains for future work to assess possible sources such as, for example, a thin partial melt layer, chemical reactions between the core and mantle (see Jeanloz, 1993), a 'graveyard' for old slabs, or a possible CMB plume source. Neither SKS, nor S2KS, nor SP_dKS are very sensitive to a possible D″ discontinuity (see Lay and Helmberger, 1983) in either V_P or V_S. For this reason, it is be difficult to relate D″ discontinuity structure to our proposed zone of reduced velocities. It will be left for future work to relate the thickness and existence of a discontinuous D″ layer to that of the basal layer we present here. For example, how does the existence of the slow basal layer beneath the southwest Pacific relate to a relatively thin (180 km) discontinuous D″ layer (Garnero et al., 1993b), and conversely, how does the possible nonexistence of a slow basal layer relate to thicker (and variable, 130–240 km) D″ layer (Young and Lay, 1990; Lay and Young, 1991; Vidale and Benz, 1993)? Including information from the P- and S-wave train at shorter distances, particularly near core-grazing distances, may help answer these questions.

6. Conclusions

A correlation between the differential times $T_{S2KS-SKS}$ and $T_{SP_dKS-SKS}$ is apparent for a small sample of well-recorded earthquakes in the southwest Pacific. When S2KS is delayed relative to SKS, so is SP_dKS. Also apparent for data displaying anomalously large $T_{S2KS-SKS}$ and $T_{SP_dKS-SKS}$ values are anomalously large and delayed SV_{diff} arrivals. Large $\delta T_{S2KS-SKS}$ residuals (with respect to PREM) can be explained by long-wavelength lower-mantle slow V_S anomalies. Large $\delta T_{SP_dKS-SKS}$ residuals, on the other hand, are explained by a thin V_P low-velocity layer at the base of the mantle. The anomalously large SV_{diff} amplitudes can be fitted with a similar thin low-velocity layer in V_S. Our data do not constrain exact features of such a basal layer, and the reduction in velocity necessary to match observations trades-off with the thickness of the layer. A scenario compatible with our observations has the following features: a 5–10% V_P and V_S low-velocity layer at the base of the mantle, smoothly or discontinuously distributed over 20–100 km (e.g. a 10% discontinuous reduction over 20 km will trade-off with a 5% smooth reduction over 100 km); overlying large-scale (1000 km or more) heterogeneous reductions in V_P and V_S (2–4%). The location of this proposed model coincides with the very slow lower-mantle shear velocities in SH12_WM13 beneath the southwest Pacific. Regions to the north, as sampled by the Indonesian data, are compatible with the global average model PREM. Smaller-scale (approximately 100 km) heterogeneity near and within the thin LVZ at the base of the mantle may explain the observed scatter in the $T_{S2KS-SKS}$ and $T_{SP_dKS-SKS}$ values and will be explored in detail in future efforts.

Acknowledgments

We thank Jeroen Ritsema, Annie Souriau, John Vidale, and Michael Wysession for helpful reviews and comments, and Steve Grand for software, data, and helpful discussions. This research was supported by NSF Grant EAR-9316441. E.J.G. was also supported by an NSF EAR Post-

doctoral Fellowship. This paper is Contribution 271, Institute of Tectonics, and Contribution 5476, Division of Geological and Planetary Sciences, California Institute of Technology.

References

Bataille, K., Wu, R.-S. and Flatte, S.M., 1990. Inhomogeneities near the core–mantle boundary evidenced from scattered waves: a review. Pageoph, 132: 151–173.

Choy, G.L., 1977. Theoretical seismograms of core phases calculated by frequency-dependent full wave theory, and their interpretation. Geophys. J. R. Astron. Soc., 51: 275–312.

Choy, G.L. and Richards, P.G., 1975. Pulse distortion and Hilbert transformation in multiply reflected and refracted body waves. Bull. Seismol. Soc. Am., 65: 55–70.

Choy, G.L., Cormier, V.F., Kind, R. and Richards, P.G., 1980. A comparison of synthetic seismograms of core phases generated by the full wave theory and by the reflectivity method. Geophys. J. R. Astron. Soc., 61: 21–39.

Dziewonski, A.M., 1984. Mapping the lower mantle: determination of lateral heterogeneity in P velocity up to degree and order 6. Geophys. J. Int., 89: 5929–5952.

Dziewonski, A.M. and Anderson, D.L., 1981. Preliminary reference Earth model (PREM). Phys. Earth Planet. Inter., 25: 297–356.

Forte, A.M., Dziewonski, A.M. and Woodward, R.L., 1993. Ashperical structure of the mantle, tectonic plate motions, nonhydrostatic geoid, and topography of the core–mantle boundary. Geophys. Monogr. Am. Geophys. Union, 72.

Garnero, E.J. and Helmberger, D.V., 1993. Travel times of S and SKS: implications for 3-D lower mantle structure. J. Geophys. Res., 98: 8225–8241.

Garnero, E.J. and Helmberger, D.V., 1994a. Evidence for correlated P- and S-wave anomalies in the lower mantle beneath the Pacific (abstract). Eos Trans. Am. Geophys. Union, 75: 663.

Garnero, E.J. and Helmberger, D.V., 1995. On seismic resolution of lateral heterogeneity in the Earth's outermost core. Phys. Earth Planet. Inter., 88: 117–130.

Garnero, E.J., Grand, S.P. and Helmberger, D.V., 1993a. Low P-wave velocity at the base of the mantle. Geophys. Res. Lett., 20: 1843–1846.

Garnero, E.J., Grand, S.P. and Helmberger, D.V., 1993b. Preliminary evidence for a lower mantle shear wave velocity discontinuity beneath the central Pacific. Phys. Earth Planet. Inter., 79: 335–347.

Garnero, E.J., Helmberger, D.V. and Grand, S.P., 1993c. Constraining outermost core velocity with SmKS waves. Geophys. Res. Lett., 20: 2463–2466.

Hales, A.L. and Roberts, J.L., 1971. The velocities in the outer core. Bull. Seismol. Soc. Am., 61: 1051–1059.

Helmberger, D.V., Zhao, L.-S. and Garnero, E.J., 1995. Construction of synthetics for 2D structures; core phases. Soc. Italiana di Fisica, in press.

Jeanloz, R., 1993. Chemical reactions at the Earth's core–mantle boundary: summary of evidence and geomagnetic implications. Jeffreys Volume, Geophys. Monogr. Am. Geophys. Union, 76: 121–127.

Kendall, J.-M. and Shearer, P.M., 1994. Lateral variations in D″ thickness from long-period shear-wave data. J. Geophys. Res., 99: 11575–11590.

Kind, R. and Müller, G., 1975. Computations of SV waves in realistic Earth models. J. Geophys., 41: 149–172.

King, S.D. and Masters, G., 1992. An inversion for radial viscosity structure using seismic tomography. Geophys. Res. Lett., 19: 1551–1554.

Krüger, F., Weber, M., Scherbaum, F. and Schlittenhardt, J., 1995. Evidence for normal and inhomogeneous lowermost mantle and core–mantle boundary structure under the arctic and northern Canada. Geophys. J. Int., in press.

Lay, T. and Helmberger, D.V., 1983. A lower mantle S-wave triplication and the shear velocity structure of D″. Geophys. J. R. Astron. Soc., 75: 799–838.

Lay, T. and Young, C.J., 1990. The stably-stratified outermost core revisited. Geophys. Res. Lett., 17: 2001–2004.

Lay, T. and Young, C.J., 1991. Analysis of SV waves in the core's penumbra. Geophys. Res. Lett., 18: 1373–1376.

Liu, X.-F. and Dziewonski, A.M., 1994. Lowermost mantle shear wave velocity structure (abstract). Eos Trans. Am. Geophys. Union, 75: 663.

Maupin, V., 1995. On the possibility of anisotropy in the D″ layer as inferred from the polarisation of diffracted S-waves. Phys. Earth Planet. Inter., in press.

Nataf, H.-C. and Houard, S., 1993. Seismic discontinuity at the top of D″: a world-wide feature? Geophys. Res. Lett., 20: 2371–2374.

Ruff, L.J. and Helmberger, D.V., 1982. The structure of the lowermost mantle determined by short-period P-wave amplitudes. Geophys. J. R. Astron. Soc., 68: 95–119.

Schweitzer, J., 1990. Untersuchung zur Geschwindigkeitsstruktur im unteren Erdmantel und im Bereich der Kern–Mantel-Grenze unterhalb des Pazifiks mit Scherwellen. Ph.D. Thesis, Frankfurt University, 134 pp.

Schweitzer, J. and Müller, G., 1986. Anomalous difference traveltimes and amplitude ratios of SKS and SKKS from Tonga–Fiji events. Geophys. Res. Lett., 13: 1529–1532.

Silver, P. and Bina, C.R., 1993. An anomaly in the amplitude ratio of SKKS/SKS in the range 100–108° from portable teleseismic data. Geophys. Res. Lett., 20: 1135–1138.

Souriau, A. and Poupinet, G., 1991. A study of the outermost liquid core using differential travel times of the SKS, SKKS, and S3KS phases. Phys. Earth Planet. Inter., 68: 183–199.

Stevenson, D.J., 1987. Limits on lateral density and velocity variations in the Earth's outer core. Geophys. J. R. Astron. Soc., 88: 311–319.

Su, W.-J., Woodward, R.L. and Dziewonski, A.M., 1994. Degree 12 model of shear velocity heterogeneity in the mantle. J. Geophys. Res., 99: 6945–6980.

Tanaka, S. and Hamaguchi, H., 1993. Velocities and chemical stratification in the outermost core, J. Geomagn. Geoelectr., 45: 1287–1301.

Vidale, J.E. and Benz, H.M., 1993. Seismological mapping of fine structure near the base of the Earth's mantle. Nature, 361: 529–532.

Vinnik, L.V., Farra, V. and Romanowicz, B., 1989. Observational evidence for diffracted SV in the shadow of the Earth's core. Geophys. Res. Lett., 16: 519–522.

Vinnik, L.V., Romanowicz, B. and Makeyeva. L., 1995. Long-range propagation of SV-diff in the D″ layer. Geophys. Res. Lett., in press.

Wysession, M.E., Okal, E.A. and Bina, C.R., 1992. The structure of the core–mantle boundary from diffracted waves. J. Geophys. Res., 97: 8749–8764.

Young, C.J. and Lay, T., 1989. The core shadow zone boundary and lateral variations of the P velocity structure of the lowermost mantle. Phys. Earth Planet. Inter., 54: 64–81.

Young, C.J. and Lay, T., 1990. Multiple phase analysis of the shear velocity structure in the D″ region beneath Alaska. J. Geophys. Res., 95: 17385–17402.